ECOSYSTEM ECOLOGY - ORIGINAL PAPER

# A universal airborne LiDAR approach for tropical forest carbon mapping

Gregory P. Asner · Joseph Mascaro · Helene C. Muller-Landau ·
Ghislain Vieilledent · Romuald Vaudry · Maminiaina Rasamoelina ·
Jefferson S. Hall · Michiel van Breugel

**Abstract** Airborne light detection and ranging (LiDAR) is fast turning the corner from demonstration technology to a key tool for assessing carbon stocks in tropical forests. With its ability to penetrate tropical forest canopies and detect three-dimensional forest structure, LiDAR may prove to be a major component of international strategies to measure and account for carbon emissions from and uptake by tropical forests. To date, however, basic ecological information such as height–diameter allometry and stand-level wood density have not been mechanistically incorporated into methods for mapping forest carbon at regional and global scales. A better incorporation of these structural patterns in forests may reduce the considerable time needed to calibrate airborne data with ground-based forest inventory plots, which presently necessitate exhaustive measurements of tree diameters and heights, as well as tree identifications for wood density estimation. Here, we develop a new approach that can facilitate rapid LiDAR calibration with minimal field data. Throughout four tropical regions (Panama, Peru, Madagascar, and Hawaii), we were able to predict aboveground carbon density estimated in field inventory plots using a single universal LiDAR model ($r^2 = 0.80$, RMSE = 27.6 Mg C ha$^{-1}$). This model is comparable in predictive power to locally calibrated models, but relies on limited inputs of basal area and wood density information for a given region, rather than on traditional plot inventories. With this approach, we propose to radically decrease the time required to calibrate airborne LiDAR data and thus increase the output of high-resolution carbon maps, supporting tropical forest conservation and climate mitigation policy.

**Keywords** Biomass · Carbon emissions · Forest carbon · Light detection and ranging · Rain forest · REDD · Remote sensing

G. P. Asner (✉) · J. Mascaro
Department of Global Ecology, Carnegie Institution for Science,
260 Panama Street, Stanford, CA 94305, USA
e-mail: gpa@stanford.edu

J. Mascaro · H. C. Muller-Landau · J. S. Hall · M. van Breugel
Smithsonian Tropical Research Institute,
Apartado Postal 0843-03092, Panama, Republic of Panama

G. Vieilledent
CIRAD, UR105 Forest Ecosystem Goods and Services,
TA C-105/D, Campus de Baillarguet,
34398 Montpellier Cedex 5, France

G. Vieilledent
DRP Forêt et Biodiversité, BP 853, Antananarivo, Madagascar

R. Vaudry
GoodPlanet Foundation, Carrefour de Longchamp,
75116 Paris, France

M. Rasamoelina
World Wide Fund for Nature, BP 738, Antananarivo,
Madagascar

## Introduction

Tropical forest structure and composition vary with climate, geological substrate, soil fertility, vegetation type, and both natural and anthropogenic disturbance regimes. These and still other factors impart enormous spatial and temporal variability in aboveground carbon density (ACD;

units of Mg C ha$^{-1}$), which is exceedingly difficult to capture using field measurements alone. Spatial and temporal variation in ACD is important from both traditional ecological and contemporary climate-change perspectives: standing carbon stocks are an integrative outcome of biological, hydrological, biogeochemical, and other functional processes (Schimel 1995); and protecting and increasing forest carbon represents a major opportunity to help offset carbon emissions that contribute to climate change. To facilitate this, the United Nations Framework Convention on Climate Change (UNFCCC) recently agreed to include provisions for reduced emissions from deforestation and forest degradation (REDD) (Herold and Skutsch 2011). As a result, there is a growing need for highly accurate, large-scale mapping of the variation and changes in forest ACD.

Light detection and ranging (LiDAR), an active remote sensing technology that uses emitted laser pulses to measure distances between objects, has proven useful for extending plot-level ACD estimates to larger spatial and ecological scales (see the review by Lefsky et al. 2002b). Most LiDAR-based work has involved airborne scanning systems that produce image-like coverage of canopy height and three-dimensional canopy metrics. LiDAR measurements have proven to be correlated with basal area (i.e., cross-sectional stem area per sample area; m$^2$ ha$^{-1}$), owing to the volumetric nature of the 3-D measurements (e.g., Drake et al. 2003; Lefsky et al. 1999b; Means et al. 1999; Popescu et al. 2004). Most work has focused on conifer, temperate broadleaf and plantation forests, with less research in tropical forests containing hundreds to thousands of canopy species (but see Drake et al. 2002; Lefsky et al. 2005).

The combination of decreased sampling time and far more robust sampling of large heterogeneous tropical regions makes LiDAR a potentially ideal platform for mapping forest carbon in support of conservation, management, and climate change mitigation programs (Asner 2009). Yet, tropical forests vary widely in structure, architecture, and composition, and the influence of these ecological properties on the efficacy of airborne LiDAR for carbon mapping has not been evaluated across a wide range of forest types and compositions. Three basic structural factors describe the amount of carbon stored aboveground in all forests: basal area (BA), height (H) and wood density (WD). Evolutionary and environmental factors create known regional-scale variation in and among these structural properties relating to carbon stocks. Recent synthesis work indicates that the ratio of tree height to diameter (H:D) varies with climate regime and forest type in the tropics (Feldpausch et al. 2010). Asian, African, and Guayana Shield forests maintain high H:D ratios, but these ratios are lower in Amazonian and Australian forests. Other synthesis work shows that WD varies regionally in tropical

forests (Baker et al. 2004; Chave et al. 2006, 2009; ter Steege et al. 2006), yet this and other ecologically based information has not been mechanistically incorporated into methods for mapping forest carbon at regional and global scales.

Despite the potential value of creating generalized LiDAR approaches for tropical forests, little work has been done to seek common ground among LiDAR metrics and field-based measures of BA, H:D, and WD. We compiled and analyzed airborne LiDAR and field plot data from recent studies spanning four distinct tropical ecoregions, including Mesoamerican forests, western Amazonian forests, Paleotropical forests of Madagascar, and Pacific island forests. Our previous studies calibrated airborne LiDAR measurements against field-based ACD estimates within regions, using comparable methods across projects (Asner et al. 2010, 2011a, b; Mascaro et al. 2011a). The results show that field-measured carbon stocks are consistently related to LIDAR measurements, but the slope of the relationship varies among regions. These differences highlight the need to explore a more general approach for the use of LiDAR in tropical forest carbon monitoring. We had two specific goals: (1) to evaluate the relative importance of different forest structural properties determining the relationship between LiDAR measurements and carbon stocks within and among different tropical forests, and (2) to develop generalized LiDAR approaches for mapping carbon stocks throughout tropical forests.

## Materials and methods

### Site descriptions

We compiled LiDAR and field data for four tropical regions: Hawaii Island, Madagascar, Amazonian Peru, and Central Panama. The regions span a wide range of climate, soil, and floristic composition, and considerable variation also exists within each region. On Hawaii Island, dry to wet tropical forests range from 180 to 11,000 mm mean annual precipitation and cover a variety of lava flows of differing ages (0 to more than 100,000 years old) and corresponding degrees of soil development. The native flora is primarily endemic (Wagner et al. 1999), with nearly all native forests containing *Metrosideros polymorpha* and/or *Acacia koa*, although much of the island's forests are now co-dominated by introduced species (Mascaro et al. 2008). The tropical moist forests in southeastern Madagascar ($\sim$2,500 mm mean annual precipitation) occupy undulating topography with steep ridges. Like those in Hawaii, the moist forests of Madagascar include a large complement of endemic species, but are infused with a Paleotropical flora due to their proximity to the African mainland (Ganzhorn

et al. 2001). The Neotropical regions of Central Panama and southern Amazonian Peru are similar in many respects, including mean annual precipitation ($\sim$2500 mm), but they differ considerably in edaphic characteristics and species composition. Madre de Dios in Peru is a region of lowland Amazonian forest abutting the Andes, which covers vast areas of highly leached tertiary substrates to fertile alluvial deposits, variously harboring tall forest hardwoods as well as bamboo- and palm-dominated stands (Gentry 1988). In Central Panama, we sampled in relatively fertile volcanic soils in the Barro Colorado Nature Monument (Leigh et al. 1982), as well as highly leached oxisols in the Agua Salud watershed adjacent to Sobernia National Park (Turner and Engelbrecht 2011). Within each region, our sampling included forests of many successional stages, from newly reverted secondary regrowth to mature forests that have been largely undisturbed for centuries (Asner et al. 2010, 2011a, b; Breugel et al. 2011; Mascaro et al. 2011a; Vieilledent et al. 2011).

Airborne LiDAR

The LiDAR data were collected using the Carnegie Airborne Observatory (CAO) Alpha system (Asner et al. 2007), with data collection and analysis methods applied consistently across sites. The CAO-Alpha LiDAR system was capable of four returns per pulse, with the beam divergence customized to 0.56 mrad. The system was operated at 2,000 m above ground level with 1.12 m spot spacing, a 30° field of view, and a pulse repetition frequency of 50 kHz, for which the aircraft maintained a ground speed ≤157 kph. Flights were planned with 100% repeat coverage (50% overlap of each swath with each adjacent swath) and therefore LiDAR point density averaged two points per 1.12 m spot. LiDAR spatial errors were less than 0.15 m vertically and 0.36 m horizontally (Asner et al. 2007, 2009).

Structural properties of forests and other woody ecosystems were estimated from these LiDAR data. Vertical canopy profiles were analyzed by binning discrete LiDAR returns into volumetric pixels (voxels) of 5 m spatial resolution and 1 m vertical resolution, yielding histograms representing the vertical distribution of vegetation in each $5 \times 5$ m spatial cell. These data were further reduced to mean canopy profile height, also known as MCH, which is the vertical center of the canopy volumetric profile (as opposed to simple top-of-canopy height). Each field-plot ACD estimate (discussed below) was then linked with a single LiDAR MCH value determined as the average MCH of all $5 \times 5$ m cells for which the center was contained within that plot's footprint (which varied in size from 0.1 to 0.36 ha across projects; Table 1). Plot size has a strong influence on the model error (RMSE), with larger plots typically resulting in lower errors, although above 0.1 ha there is little influence on model coefficients (Mascaro et al. 2011b). Across projects with plots of many sizes, MCH exhibits a strong relationship with forest structural properties such as basal area and carbon density (e.g., Asner et al. 2010; Lefsky et al. 1999a, 2002a; Mascaro et al. 2011a).

Field data

Within each region, we developed ground-based estimates of aboveground carbon density across a range of habitat types using inventory plots and allometric equations

**Table 1** Key statistics on the field plot data for humid tropical forests in the Peruvian Amazon, Panama, Madagascar, and Hawaii

| Region | Number and size of plots | Plot shape | Taxonomic resolution | Mean (SD) characteristics of closed forest sites (MCH >15 m) | | | References |
|---|---|---|---|---|---|---|---|
| | | | | Carbon density (Mg ha$^{-1}$) | Basal area (m$^2$ ha$^{-1}$) | Wood density (g cm$^{-3}$) | |
| Peru | 130 (0.28 ha) | Circular | Genus | 135 (46) | 33 (7) | 0.56 (0.05) | Asner et al. (2010) |
| Panama | 128 (0.36 ha) | 60 × 60 m | Species | 113 (28) | 32 (6) | 0.54 (0.03) | Mascaro et al. (2011a) |
| | 29 (0.1 ha) | 20 × 50 m | | | | | |
| Madagascar | 46 (0.28 ha) | Circular[a] | Species | 144 (49) | 42 (11) | 0.58 (0.03) | Asner et al. (2011b) |
| Hawaii | 83 (0.28 ha) | Circular | Species | 237 (58) | 56 (12) | 0.65 (0.03) | Asner et al. (2011a) |
| | 36 (0.1 ha) | Circular | | | | | |
| | 30 (0.18 ha) | Circular | | | | | |

The data span nonplanted intact mature forests, secondary and degraded forests, logged forests, and open woodlands, as described in the references. To allow a comparison among sites, the mean and standard deviation (SD) of aboveground carbon density, basal area, and wood density above a LiDAR mean canopy profile height (MCH) of 15 m are also provided. In general, forests with an MCH >15 have achieved canopy closure

[a] Plots in Madagascar were nested: trees >50 cm were sampled inside a 30 m radius (0.28 ha), those >20 cm inside a 14 m radius, and all others inside a 4 m radius

relating stem diameter, height, and wood density to stem biomass (IPCC 2006). For each region, a detailed accounting of the specific methods is available in the original publications (Asner et al. 2010, 2011a, b; Mascaro et al. 2011a; Vieilledent et al. 2011). The plot sampling was designed specifically to capture the range of possible structural variation encountered by the sensor. Importantly, however, the field plots did not (and were not intended to) represent a random sample of forest structural variation at the landscape scale. Rather, to capture the relationship between LiDAR and forest structure requires uniform sampling along the range of possible structural conditions—whether they are common (e.g., median forest height) or rare (e.g., low forest height). Thus, field plots for all four regions targeted nonplanted forest stands of all ages, from mature stands to recently abandoned pasture with few trees and, in the case of Hawaii, open savannas on primary successional lava flows. We did not discriminate between uneven- and even-aged stands, although uneven-aged stands were the norm for mature forests outside of Hawaii (where even-aged stands of the native dominant *Metrosideros polymorpha* senesce and regenerate in synchrony; Wagner et al. 1999). Plot size, shape, and spacing differed according to the various goals (and limitations) of the respective projects (Table 1). In Hawaii and Madagascar, sampling was planned based on a prior examination of structural variation found in the LiDAR data (e.g., to locate exceptionally tall or short forests); in Peru, the sampling was planned based on known habitat variation from previous vegetation surveys; in Panama, we utilized pre-existing plots.

In all cases, we estimated biomass by allometric regression using, with decreasing priority depending on which models were available, (1) species-specific equations, (2) growthform-specific equations (i.e., lianas, palms, bamboo, tree ferns), (3) generalized regional equations (Breugel et al. 2011; Vieilledent et al. 2011), and finally (4) pan-tropical equations (Chave et al. 2005). For equations with a wood density term, we utilized, with decreasing priority, (1) local field-sampled estimates by species, (2) species-level database estimates (Chave et al. 2009), (3) genus-level database estimates, and (4) regional estimates (Chave et al. 2006). In general, the biomass of most stems was estimated with a taxon-assigned wood density value, but by a general (rather than species-specific) allometric model. In Hawaii, where many species-specific models were available, we found that predicted biomass from species-specific versus general models differed for a given stem, but that the net effect on total plot-level biomass was small (Asner et al. 2011a).

The compiled field measurements highlight similarities and differences among forests over a given MCH range (Table 1). In plots above an MCH of 15 m, ACD ranges from 135 ($\pm$46) Mg C ha$^{-1}$ in the Peruvian Amazon to 237 ($\pm$58) Mg C ha$^{-1}$ in native Hawaiian forests. Mean basal area (BA) and wood density track mean carbon density across regions (Table 1).

Regional vs. universal models

Our approach to developing a universal model to relate LiDAR MCH to field-measured ACD (Mg ha$^{-1}$) draws on recent efforts to develop generalized biomass allometries for tropical trees (Chave et al. 2005), and those warrant review here. For a given tree species, dry aboveground biomass (AGB, of which $\sim$48% is carbon) can be related to tree diameter ($D$), ideally in the form of a power function,

$$AGB = aD^b \tag{1}$$

(Niklas 2006). However, such models show less utility when they include many species, due to differences in tree form (e.g., taper as well as the height–diameter allometry) and wood density (which varies by an order of magnitude among tropical tree species). In contrast, generalized models are trivariate, incorporating diameter, height, and wood density terms. Together, these variables collectively explain about 95% of the variation in the logarithm of tropical tree biomass (Chave et al. 2005). The simplest form is

$$AGB = aD^{b_1}H^{b_2}WD^{b_3}, \tag{2}$$

where $H$ is height and WD is wood density. To date, regional models relating ACD and LiDAR metrics have been univariate, relying primarily on MCH or related indices (e.g., Lefsky et al. 1999b), and taking a form similar to Eq. 1:

$$ACD = aMCH^b. \tag{3}$$

Here, LiDAR-measured MCH is related to field-measured ACD. Just as with an allometric relationship between diameter and biomass for a single tree species (e.g., Eq. 1), these models are highly conserved within a region, but are not consistent across regions. Although the regional models include information on forest canopy vertical profile, they lack parameters that may differ among forests with similar height profiles. Specifically, they lack information on tree diameters and stocking (e.g., stem density), which together are integrated as BA, as well as WD.

We considered how differences in plot-level BA–MCH relationships, plot-level WD–MCH relationships, and tree height–diameter allometries may contribute to differing MCH-to-ACD models among regions. We evaluated how plot-level BA (total basal area for stems $\geq$1 cm dbh per area of ground) and plot-level WD (a per-plot average as weighted by each stem's BA contribution) related to LiDAR MCH within each region using linear regression by

ordinary least squares, and compared the relationships among regions. We also compared allometric models relating height to diameter (e.g., Chave et al. 2005), henceforth referred to as *H:D* models, among regions. These models were previously constructed using up to third-order polynomials fitted to ln-transformed diameter and height data. Within certain regions, such as Hawaii, species-specific models were used; however, within most regions we relied on a single generalized model because there were insufficient data to parameterize species-specific models for all relevant species.

Extending tree allometry theory to the plot scale, we devised the following general model of plot-based ACD:

$$\text{ACD} = a\text{MCH}^{b_1}\text{BA}^{b_2}\text{WD}_{\text{BA}}^{b_3}, \tag{4}$$

where BA is basal area and $\text{WD}_{\text{BA}}$ is the basal-area-weighted wood density of each plot. The model was fitted using multiple linear regression on ln-transformed plot-level data for MCH, BA, and $\text{WD}_{\text{BA}}$ in the form

$$\ln(\text{ACD}) = \ln(a) + b_1\ln(\text{MCH}) + b_2\ln(\text{BA}) + b_3\ln(\text{WD}_{\text{BA}}). \tag{5}$$

We then back-transformed the final model and multiplied by a correction factor (CF) to account for the back-transformation of the regression error (Baskerville 1972); the correction factor is given by $\text{CF} = e^{\text{MSE}/2}$, where MSE is the mean square error of the regression model. We evaluated how the predictive power of this model changed when we used regional average wood density instead of plot level wood densities, and when we used regional BA:MCH slopes times observed plot MCH in place of observed plot BA. Our final universal model incorporated plot-level data on MCH, regional average wood density, and regional BA:MCH slopes. We compared the performance of this universal model to each previously published regional ACD:MCH model in terms of their match to the observed carbon density by fitting linear regressions between observed and predicted carbon density, and also by calculating $r^2$ values, mean errors, and RMSE.

## Results

### Relating LiDAR to canopy structure and carbon stocks

Sample LiDAR cross-sections taken from the four regions, along with the mean and spatial variance of the vertical distribution of canopy elements such as leaves and stems, are shown in Fig. 1. Visual comparison of the vertical canopy profiles revealed general consistency among Panama, Peru, and Madagascar, but Hawaii is very much an
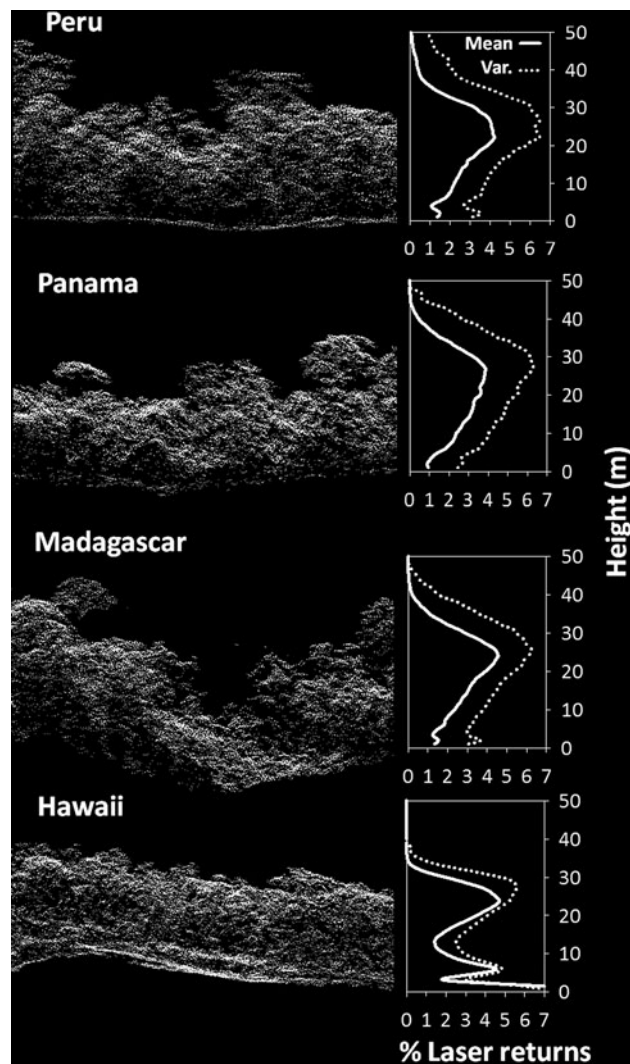


**Fig. 1** LiDAR cross-sectional views of four mature tropical forests in the Peruvian Amazon (Los Amigos Conservation Concession, Madre de Dios), Panamanian Neotropics (Barro Colorado Island), Paleotropics (southeastern Madagascar), and Pacific island forests (Laupahoehoe Forest Reserve, Hawaii Island). Each cross-section shows the three-dimensional structure of the forest in a 100 m long × 20 m wide belt transect. *Right-hand panels* show mean and spatial variance of LiDAR vertical canopy profiles for all returns in a 1 km² area centered on each cross-section. The mean canopy profile height (MCH) is established as the vertical center of the canopy volumetric profile

outlier. It has a shorter canopy, with a narrower upper tail in its vertical distribution, likely indicating fewer emergent trees that are clearly visible at the other sites. The Hawaii profile also contains a dense and distinctive understory layer (~7 m in height) and dense groundcover layer (1–2 m), and while the other sites contain understory and groundcover vegetation, the layering is not nearly as well stratified. All sites contain a mode centered near 20 m in

Fig. 2 Comparison of regionally derived relationships between LiDAR mean canopy profile height (MCH) and plot-level estimates of aboveground carbon density (ACD) generated by stand information including tree diameters, heights, and species/genus-specific wood densities. Panels **a–d** are for each forest ecoregion; **e** provides the data spread among all ecoregions; **f** compares regression lines among ecoregions. Regression parameters are provided in the ESM. The *horizontal line* indicates the approximate MCH level for each example stand shown in Fig. 1. *Symbols* for each forest ecoregion are consistently presented in Figs. 2, 3, 4, 5, and 6
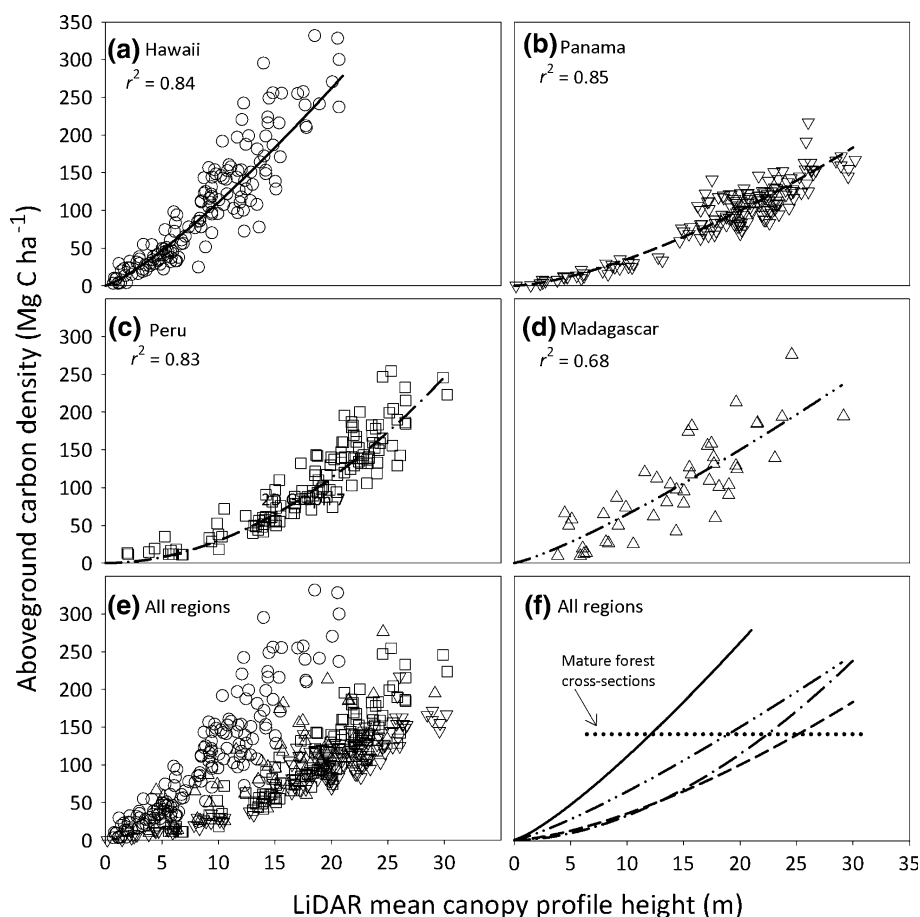


height; it is in this area that the greatest density of canopy elements can be found in all four forests.

As documented in our studies of each of these regions, aboveground carbon density can be predicted with high confidence from LiDAR-derived MCH within a particular region (Fig. 2). The proportion of variation explained by the MCH-to-ACD regressions was roughly similar across regions ($r^2$ = 0.68–0.85, RMSE = 18–36 Mg C ha$^{-1}$; Fig. 1a–d), but the slope of the relationship varied twofold (Fig. 2e). Hawaiian forests diverged the most from Neotropical forests in Peru and Panama, while Madagascar fell between these extremes (Fig. 2f). A summary of all model parameters is provided in the Electronic supplementary material (ESM). Relative plot size and quality was a factor in the various model fits; the nested plots used in Madagascar (Table 1) contributed to their higher RMSE (Fig. 2f), while the largest plots (used in Panama) were associated with the lowest RMSE (Fig. 2b; see also Mascaro et al. 2011b).

Basal area was highly and linearly correlated with LiDAR MCH in all four regions (Fig. 3). However, the mean basal area of each forest at a given MCH differed between regions, which is reflected in the pronounced variation in the basal area of closed-canopy forests (MCH >15 m) across regions. Closed-forest basal area declined steadily from Hawaii

(mean 56 m$^2$ ha$^{-1}$), to Madagascar (45 m$^2$ ha$^{-1}$), to the Neotropics (32–33 m$^2$ ha$^{-1}$; Table 1). There were corresponding declines in the steepness of the MCH-to-ACD slopes observed in Fig. 2.

Plot-level, BA-weighted average WD had no consistent relationship with MCH among regions (Fig. 4). MCH and WD were weakly positively correlated in Peru, very weakly negatively correlated in Hawaii and Panama, and had no significant correlation in Madagascar. The positive relationship in Peru reflects the fact that mature forest plots had higher WD on average than plots in young, regenerating stands. Somewhat surprisingly, the same was not true for the other regions. However, WD did vary considerably across regions. In Hawaii, most field plots were centered on a WD of 0.69—the value of the widespread dominant tree *Metrosideros polymorpha*. With the exception of a single plot in Madagascar, all plots in the other regions had WD values of less than 0.69. Among plots in mature forests, WD was 14–17% lower in Neotropical regions of Peru (mean = 0.55 g cm$^{-3}$) and Panama (0.54 g cm$^{-3}$) and 11% lower in Madagascar (0.57 g cm$^{-3}$) than in Hawaii (0.65 g cm$^{-3}$; Table 1). As with basal area, this sequence corresponded to the trend in the relative steepness of slopes of the LiDAR-to-ACD relationships from the various regions (Fig. 2).

**Fig. 3** Relationships between LiDAR MCH and plot-level estimates of basal area as determined by tabular tree measurements. Panels **a–d** are for each forest ecoregion; **e** provides the data spread among all ecoregions; **f** compares regression lines among ecoregions. Regression parameters are provided in the ESM
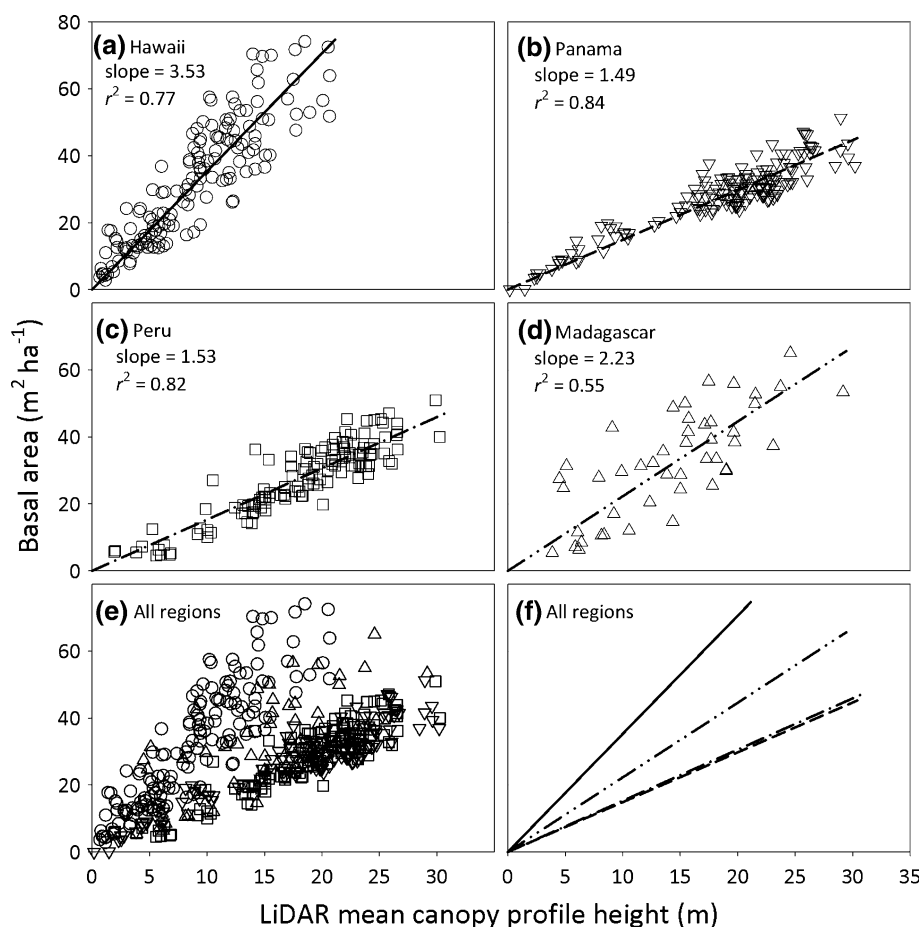


Comparing height–diameter allometries, we found that, at a given tree diameter, Neotropical trees were generally taller (particularly in Peru) than those in Madagascar, and all were far taller than those in Hawaii (Fig. 5). The regional model for Hawaii reflects the fact that the most dominant tree, *Metrosideros polymorpha*, cannot generally attain the height that mainland tropical trees reach. Overall, we find that regional variation in *H:D* relationships can drive differences in the regional MCH-to-ACD curves when BA is roughly similar. For example, MCH-to-BA curves were nearly overlapping in Panama and Peru (Fig. 3), while Peru had a slightly steeper *H:D* relationship (Fig. 5). This leads to a steeper MCH-to-ACD curve in Peru relative to Panama (Fig. 2).

Universal LiDAR-to-ACD model

Our general model incorporating plot-level MCH, BA, and WD explained 96% of the variation in log-transformed ACD among all 482 field plots. It resulted in the following equation (after back-transformation, including correction for the regression error):

$$ACD = 2.04 MCH^{0.436} BA^{0.946} WD^{0.912}. \qquad (6)$$

All terms were significant at $p < 0.001$. Standard errors for the exponents were 0.0221 for MCH, 0.0215 for BA, and 0.0832 for WD. When we applied the original plot-level field data to this final model, we obtained a linear relationship between observed and predicted ACD that explained 95% of the variation ($p < 0.0001$; Fig. 6a). The root mean squared error (RMSE) was 15 Mg C ha$^{-1}$. We then generated predictions from the same model using plot-level data only for MCH; we substituted regionally averaged wood density for plot-level wood density, and regional BA:MCH constants multiplied by the plot-level MCH for the plot-level BA. This "universal" approach explained 80% of the variation in field-measured ACD for all regions combined (RMSE = 27.6 Mg C ha$^{-1}$; $p < 0.001$; Fig. 6d). We also considered the influence of the two regional constants by including each one separately (i.e., using plot-specific data for the other). Including plot-level BA but a regional WD constant explained nearly the same variation (92%) as with the full plot-level model (95%), indicating that plot-level WD accounted for little overall variation (Fig. 6c). By contrast, using plot-level WD but a regional BA:MCH constant caused the explained variation to drop from 95% to 82% (Fig. 6b).

**Fig. 4** Relationships between LiDAR MCH and basal area-weighted wood density (WD). For a given plot, mean WD was determined as the summed product of WD and basal area for each stem divided by the summed basal area. Panels **a–d** are for each forest ecoregion; **e** provides the data spread among all ecoregions; **f** compares regression lines among ecoregions. Regression parameters are provided in the ESM
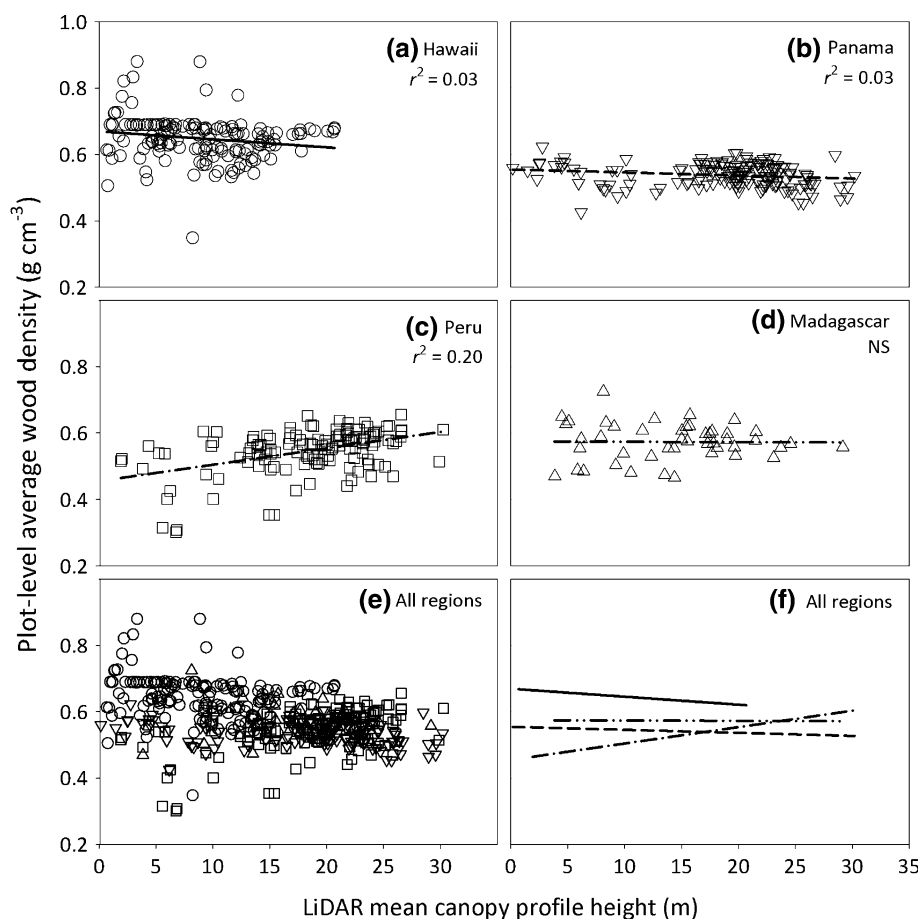


Considering each region independently, ACD variation explained by the universal model differed by a maximum of just 1% relative to region-specific models (Fig. 7). Similarly, the RMSE was essentially unchanged. Median errors by region differed by −4.2, −4.8, 4.0, and 6.2 Mg C ha$^{-1}$ for Panama, Peru, Madagascar, and Hawaii, respectively. The greatest difference in slope between regional and universal models was found in Peru, where high-ACD regions were slightly underpredicted by the universal model. The reason for these model performance differences is likely the small but statistically significant effect of increasing wood density with increasing stand-level carbon stocks in the southern Peruvian Amazon; when we apply the universal model, we lose the plot-scale contribution of wood density to the MCH-to-ACD calibration, which causes underestimation in high-biomass stands.

## Discussion

Our compilation of previous and ongoing airborne LiDAR studies finds substantial variation in the canopy structure of closed-canopy tropical forests, both within and across tropical forest ecoregions. Each of these studies purposely sampled as wide a variety of forest compositions and conditions as is known to occur in each region. Specifically, the plots include a wide range of plant species, genera and families, as well as enormous variation in successional states and disturbance conditions, ranging from nearly deforested to selectively logged to young secondary regrowth and closed-canopy intact forests (Asner et al. 2010, 2011a, b; Mascaro et al. 2011a). Furthermore, while the same airborne LiDAR and mapping approach was used in all four ecoregions, the plots were measured by different groups, and varied in plot size and detail (Table 1). From this diverse set of conditions, we were able to quantitatively compare the factors determining the relationship between LiDAR measurements (Fig. 1) and aboveground carbon density (Fig. 2). This relationship proved to be consistent in functional form but to vary in slope by ecoregion, affording an opportunity to improve our understanding of the sources of such variation.

The results presented here ultimately suggest a consistency in the way trees naturally fill tropical forest canopy space, and are thus detected by LiDAR, that is analogous to the consistency exhibited by tree allometry models (Niklas 2006). Naturally occurring (unplanted)

**Fig. 5** Relationships between field-measured tree height and diameter (*H:D*). Panels **a–d** are for each forest ecoregion; **e** provides the data spread among all ecoregions; **f** compares regression lines among ecoregions. Regression parameters are provided in the ESM
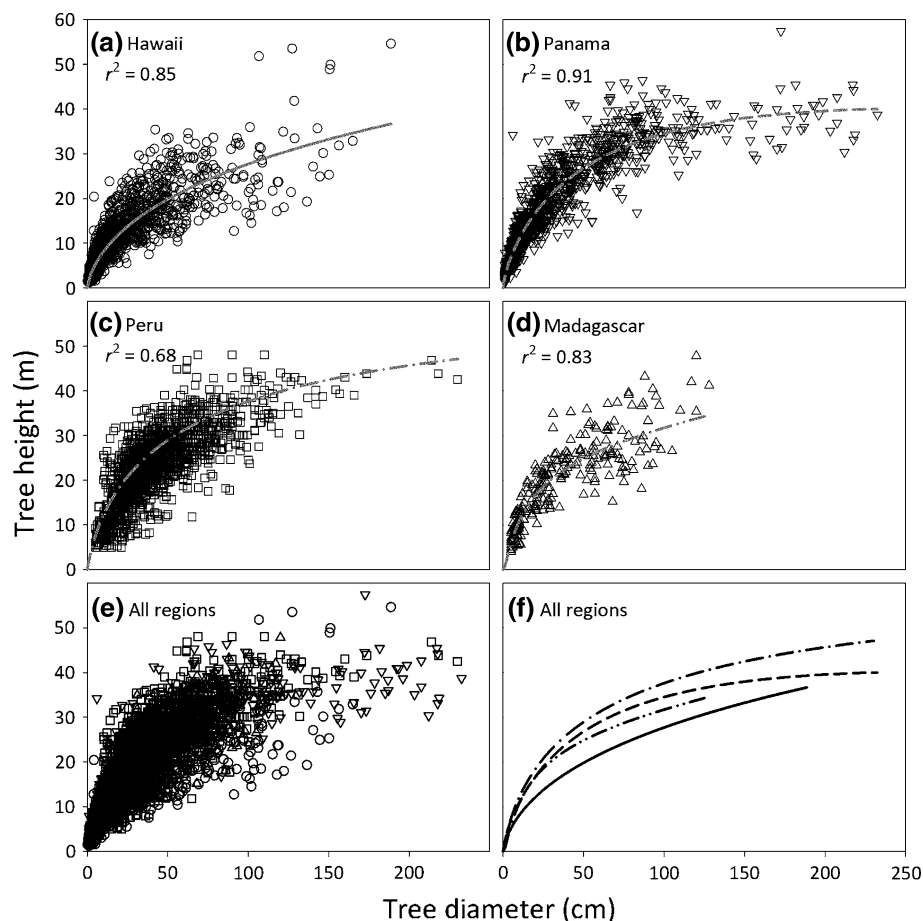


tropical forests undergo successional processes driven by competition for resources, particularly light and nutrients (Brokaw 1985; Kitajima et al. 2005). This leads to both vertical and horizontal partitioning of canopy area and structure (Enquist and Arak 1994), which, within regions, is supported by relatively predictable investments in bole wood volume and basal area to support multi-level canopy space-filling (Richards and Williamson 1975; Richards 1952). Although wood density varies regionally [with some suggesting that it alone can explain biomass variation among tropical forests (Baker et al. 2004), while other see less of a pattern (Stegen et al. 2009)], the end result can be a surprisingly convergent pattern of canopy structure and space filling among tropical forests (Kellner and Asner 2009). We have combined this thinking with high-resolution airborne LiDAR measurements of canopy structure to derive a universal approach to mapping carbon. While this approach relies on regional estimates of basal area and/or wood density to produce the most accurate mapping predictions, the consistency in the way that trees fill the canopy space is foundational. We note that this approach breaks down in plantation-type forests where spacing and height become very homogeneous. In these cases, the relationship between

LiDAR-derived canopy structure and carbon stocks loses fidelity (Asner et al. 2011a).

## Relating LiDAR to tropical forest structure and carbon stocks

In concurrence with past studies, we found strong linear relationships between airborne LiDAR measurements of canopy profile height and plot-level basal area within regions (Fig. 3). This occurs because the MCH is sensitive to the volumetric centroid of the laser point distribution in the crown, and both crown height and crown volume generally scale with stem diameter and basal area in tropical forests (e.g., Asner et al. 2002; Baker and Wilson 2000; Clark et al. 2004). Although the MCH-to-BA relationships were linear within all regions, their slopes varied more than two-fold, from the lowest observed in Central Panama to the highest in Hawaii (Fig. 3). These BA:MCH ratios generally parallel the differences observed among the MCH-to-ACD regressions (Fig. 2), but they also follow the general pattern seen in regional *H:D* models (Fig. 5). In forests with shallower *H:D* models (e.g., Hawaii), basal area necessarily must be greater at a given canopy height than in forests with steeper *H:D* models (e.g., Peru), provided they have similar stocking.

**Fig. 6** Observed aboveground carbon density versus that predicted by various iterations of the universal LiDAR approach: **a** the model fit with parameters for the LiDAR MCH, field-estimated basal area, and basal area-weighted wood density for each plot; **b** the model with regional basal area-to-MCH ratios in place of field-estimated basal area estimates, **c** the model with regional wood density constants in place of field-estimated wood density, and **d** the universal model, with both regional basal area-to-MCH ratio and regional wood density constant
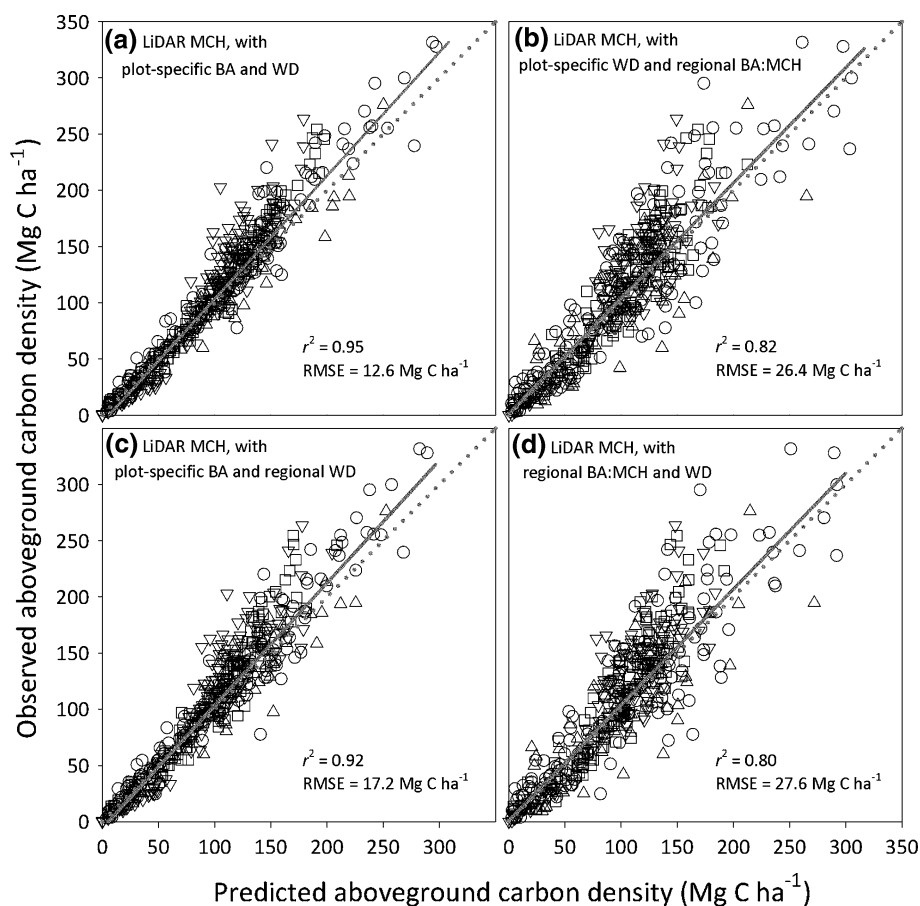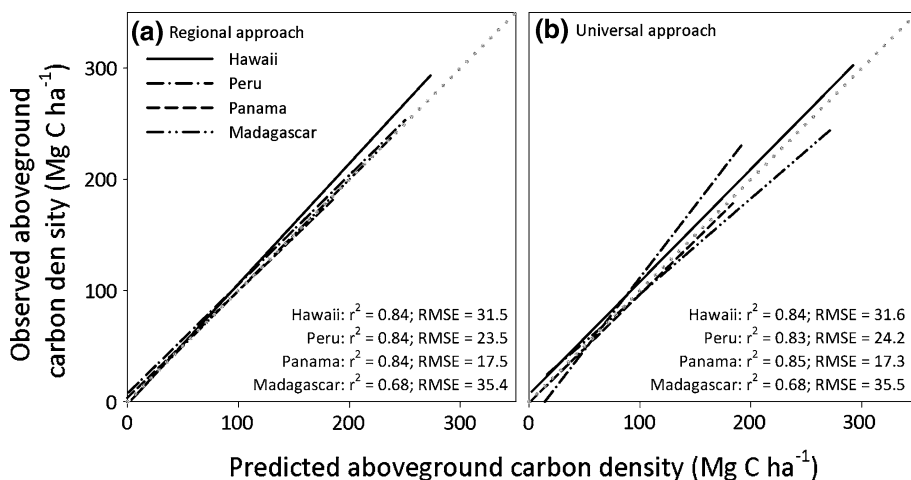


**Fig. 7** Comparison of the predicted and observed carbon densities for four tropical regions using: **a** regional models calibrated by field inventory plots, and **b** a single universal model using only LiDAR MCH, regional estimates of basal area-to-MCH ratio, and mean basal area-weighted wood density values



LiDAR cannot detect differences in wood density, and thus the extent to which wood density influences ACD variation presents a challenge to the use of LiDAR for forest carbon mapping. This issue is particularly important given potential regional variation in wood density as well as the possibility of long-term species compositional shifts resulting from local and global anthropogenic influences

(Chave et al. 2008; Schnitzer and Bongers 2011). Two key questions must be considered in the context of LiDAR efforts to map ACD: (1) how does wood density affect ACD across regions, and (2) how does wood density affect ACD within a region? This study, like previous work (Baker et al. 2004; Chave et al. 2006; Reyes et al. 1992; ter Steege et al. 2006), has shown that wood density is

correlated with ACD patterns across regions. Here, for example, we found that higher regional wood density in Hawaiian forests—and to a lesser extent Madagascar—was related to higher ACD at a given forest MCH (Table 1; Fig. 2). However, the pattern is less clear within any given region (Fig. 4). Relationships between WD and ACD were comparable in slope and goodness of fit to those between WD and MCH, showing weak positive, weak negative, or no relationships in different regions (Fig. 4; ESM). Stegen et al. (2009) also found that wood density was sometimes positively, sometimes negatively, and sometimes not correlated with ACD in six Neotropical forests. In summary, our results support a strong among-region influence of wood density on ACD, but a relatively weak influence within a region.

The universal LiDAR model (Eq. 6) explained nearly all the variation (95%) in observed ACD when it was applied to field-measured BA, field-estimated WD, and LiDAR-derived MCH for each plot (Fig. 6a). It is important to note that information on tree diameters, height, and WD feed into both axes, albeit in different forms, and thus a strong fit is not surprising. It is instructive, however, because it demonstrates that plot-specific variables explain nearly all the variation in ACD that tree-specific variables do. Thus, among-tree variation, such as the taxon-assigned wood density values, and the relative distribution of this variation among stems (e.g., which wood density values get assigned to trees of a certain BA) ultimately have very little effect on plot-specific estimates of ACD. This is a key development in the application of LiDAR to mapping tropical forest biomass because it provides a path toward rapid calibration.

For all forests, the MCH-to-ACD relationships were nonlinear, while the MCH-to-BA relationships were linear. This disparity is a consequence of the intrinsic nonlinearity between ACD and BA. For individual trees, ACD is approximately proportional to $D^2 \times H \times$ WD (Chave et al. 2005). The basal area of an individual tree is proportional to the square of its diameter, while height is also approximately a power function of diameter, with an exponent of between 0.46 and 0.65 in tropical regions (Feldpausch et al. 2010). Thus, the ACD of an individual tree is approximately proportional to $D^{2.45-2.65}$ and thus $BA^{1.22-1.33}$ in most tropical forest trees. A similar relationship holds at the stand level, with plot-level ACD related to plot-level BA density as a power function. For the sites considered in this study, ACD was proportional to $BA^{1.34}$ (see ESM).

It is notable that the four tropical regions considered here displayed balancing influences of $H{:}D$ and regional WD on aboveground carbon density. That is, the relatively short forests of Hawaii, and to a lesser extent Madagascar, also have higher wood density. This is the opposite of the pattern that might be expected from a biomechanics

perspective, in which higher wood density would enable trees to be stronger and thus taller for a given diameter, and would lead to the expectation that regions with higher wood density would also have higher $H{:}D$ (Larjavaara and Muller-Landau 2010). In the global humid tropical forest biome, several ecoregions do contain forests with both tall trees and high wood density. For example, dipterocarp forests of Southeast Asia and others in the Eastern Amazon have steeper $H{:}D$ relationships and higher wood density than the forests currently incorporated into our universal approach (Feldpausch et al. 2010; King et al. 2005). Although our universal LiDAR model would certainly estimate high ACD for these regions (consistent with field inventories in such areas), these regions introduce new uncertainty, since they do not enter into our current universal parameterization.

We caution that our results may not be applicable to some airborne LiDAR systems (e.g., large-footprint LiDAR), or to spaceborne LiDAR profilers such as the NASA Geoscience Laser Altimeter System (GLAS) (Abshire et al. 2005). While each of these approaches is capable of detecting forest height and vertical partitioning of canopy elements, neither can produce high-resolution 3-D information on the structural properties of canopies. Thus, the underlying controls over canopy space-filling revealed in the high-resolution approach described here may not be detectable using coarser airborne and spaceborne methods.

Universal LiDAR approach for tropical forests

To date, LiDAR-based carbon mapping has been dependent upon a region-specific calibration involving laborious and expensive plot inventory data, including tree diameter measurements, tree identification (for wood density estimation), and a robust set of tree height measurements (Fig. 8). This technique has been successfully employed in both temperate and tropical forest environments. However, we have found that nearly all of the variation in field-based estimates of ACD can be sufficiently captured at the plot scale using the LiDAR MCH, after accounting for inter-regional differences in wood density, and with the application of a regional BA-to-MCH correction (Fig. 8). Moreover, we found that the universal approach yields results that are comparable to regionally calibrated LiDAR-to-ACD methods (Fig. 7). With the universal approach developed here (Fig. 8), we can estimate aboveground carbon density using airborne LiDAR in combination with a minimal number of co-registered field plots for which only total basal area is measured—something that can be done rapidly with a wedge prism or relascope (Kalliovirta et al. 2005). This reduces logistical and financial investments to simple estimates of basal area at a sufficient number of points to

characterize the BA-to-MCH relationship for a given region. In practice, we have found that fewer than 25 plots of 30 m radius each spread across a range of biomass levels are sufficient to reach the same low error levels in LiDAR-to-ACD calibration as achieved with a much larger number of plots (Asner et al. 2010, 2011a). We have also found that larger size plots substantially reduce calibration model errors, such that for 1 ha calibration plots, errors decline to 10% of the mean ACD in mature forests (Mascaro et al. 2011b). Thus, the universal model RMSE of 27.6 Mg C ha$^{-1}$ reported here is conservative because relatively small plots were employed (0.1–0.36 ha).

The universal approach (Fig. 8) will be most accurate if an effort is made to tabulate the dominant genera found in the mapping region, especially among the larger, heavier canopy species dominating forest carbon stocks. This list can be developed while collecting basal area estimates. While we did find a significant relationship between wood density and carbon stocks in the Peruvian Amazon, no consistent slope angle or consistent level of explained variance existed among ecoregions (Fig. 5; see also Stegen et al. 2009). Without a consistent trend, it is our view that literature-derived estimates of regional wood density—which are now widely available for the tropics (Chave et al. 2006; Reyes

et al. 1992; ter Steege et al. 2006; Zanne et al. 2009)—can provide appropriate and practical model inputs. This perspective is further supported by the observation that wood density variation within a region has a small effect on the accuracy of LiDAR-based estimates of aboveground carbon density (Fig. 6a, c).

Combined with regional BA-to-MCH ratios and regional average wood density estimates, airborne LiDAR can provide input to yield high-resolution maps of aboveground carbon density in tropical forests without the need for laborious and time-consuming forest inventory plots within the LIDAR footprint. Our proposed universal approach represents a significant step toward the rapid production of high-resolution carbon inventories for tropical forests. In the past, ground-based biomass assessments have been the most time-consuming part of regional airborne LIDAR campaigns. With a universal approach, we propose to decrease the time required to calibrate airborne LiDAR data, and thus accelerate the production of high-resolution carbon maps in support of the monitoring and verification of carbon stocks and emissions in tropical forests.
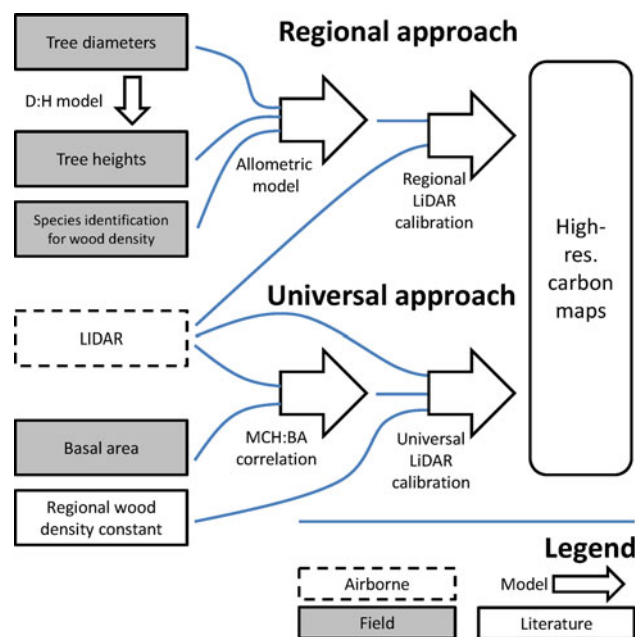
**Fig. 8** Diagram showing the input data required to produce high-resolution maps of aboveground carbon density using the traditional regional approach (*top*) and using the proposed universal approach (*bottom*). Whereas the regional approach relies on exhaustive inventories of tree diameters, heights, and species identifications in the field (for wood density estimation), the universal approach uses only field estimates of basal area to provide a regional LiDAR MCH-to-basal area conversion. This is combined with LiDAR MCH and regional wood density information to yield a final calibration allowing mapping

## References

Abshire JB et al (2005) The geoscience laser altimeter system (GLAS) on the ICESat mission: on-orbit measurement performance. Geophys Res Lett 32:L21S02

Asner GP (2009) Tropical forest carbon assessment: integrating satellite and airborne mapping approaches. Environ Res Lett 3:1748–9326

Asner GP, Palace M, Keller M, Pereira R, Silva JNM, Zweede JC (2002) Estimating canopy structure in an Amazon forest from laser range finder and IKONOS satellite observations. Biotropica 34:483–492

Asner GP et al (2007) Carnegie Airborne Observatory: in-flight fusion of hyperspectral imaging and waveform light detection and ranging (LiDAR) for three-dimensional studies of ecosystems. J Appl Remote Sens 1:013536. doi:10.1117/1111.2794018

Asner GP, Hughes RF, Varga TA, Knapp DE, Kennedy-Bowdoin T (2009) Environmental and biotic controls over aboveground biomass throughout a tropical rain forest. Ecosystems 12:261–278

Asner GP et al (2010) High-resolution forest carbon stocks and emissions in the Amazon. Proc Natl Acad Sci USA 107:16738–16742

Asner GP et al (2011a) High-resolution carbon mapping on the million-hectare Island of Hawaii. Frontiers Ecol Environ 9:434–439. doi:10.1890/100179

Asner GP et al (2011b) Multi-scale analysis of aboveground carbon storage in Madagascar. Biogeosciences (in review)

Baker PJ, Wilson JS (2000) A quantitative technique for the identification of canopy stratification in tropical and temperate forests. For Ecol Manag 127:77–86

Baker TR et al (2004) Variation in wood density determines spatial patterns in Amazonia forest biomass. Glob Change Biol 10:545–562

Baskerville G (1972) Use of logarithmic regression in the estimation of plant biomass. Can J For Res 2:49–53

Breugel MV, Ransijn J, Craven D, Bongers F, Hall JS (2011) Estimating carbon stock in secondary forests: decisions and uncertainties associated with allometric biomass models. For Ecol Manag 262:1648–1657

Brokaw NVL (1985) Treefalls, regrowth, and community structure in tropical forests. In: Pickett STA, White PS (eds) The ecology of natural disturbance and patch dynamics. Academic, New York, pp 53–69

Chave J et al (2005) Tree allometry and improved estimation of carbon stocks and balance in tropical forests. Oecologia 145:87–99

Chave J, Muller-Landau HC, Baker TR, Easdale TA, ter Steege H, Webb CO (2006) Regional and phylogenetic variation of woody density across 2456 Neotropical tree species. Ecol Appl 16:2356–2367

Chave J et al (2008) Assessing evidence for a pervasive alteration in tropical tree communities. PLoS Biol 6:e45

Chave J, Coomes D, Jansen S, Lewis SL, Swenson NG, Zanne AE (2009) Towards a worldwide wood economics spectrum. Ecol Lett 12:351–366

Clark DB, Read JM, Clark ML, Cruz AM, Dotti MF, Clark DA (2004) Application of 1-m and 4-m resolution satellite data to ecological studies of tropical rain forests. Ecol Appl 14:61–74

Drake JB, Dubayah RO, Knox RG, Clark DB, Blair JB (2002) Sensitivity of large-footprint lidar to canopy structure and biomass in a neotropical rainforest. Remote Sens Environ 81:378–392

Drake JB et al (2003) Aboveground biomass estimation in closed canopy neotropical forests using lidar remote sensing: factors affecting the generality of relationships. Glob Ecol Biogeogr 12:147–159

Enquist M, Arak A (1994) Symmetry, beauty and evolution. Nature 372:169–172

Feldpausch TR et al (2010) Height–diameter allometry of tropical forest trees. Biogeosci Discuss 7:7727–7793

Ganzhorn JU, Lowry PP, Schatz GE, Sommer S (2001) The biodiversity of Madagascar: one of the world's hottest hotspots on its way out. Oryx 35:346–348

Gentry AH (1988) Changes in plant community diversity and floristic composition on environmental and geographical gradients. Ann Mo Bot Gard 75:1–34

Herold M, Skutsch M (2011) Monitoring, reporting and verification for national REDD + programmes: two proposals. Environ Res Lett 6:014002

IPCC (2006) Guidelines for national greenhouse gas inventories. IPCC National Greenhouse Gas Inventories Programme/Institute for Global Environmental Strategies, Hayama

Kalliovirta J, Laasasenaho J, Kangas A (2005) Evaluation of the laser-relascope. For Ecol Manag 204:181–194

Kellner JR, Asner GP (2009) Convergent structural responses of tropical forests to diverse disturbance regimes. Ecol Lett 12:887–897

King DA, Davies SJ, Nur Supardi MN, Tan S (2005) Tree growth is related to light interception and wood density in two mixed dipterocarp forests of Malaysia. Funct Ecol 19:445–453

Kitajima K, Mulkey SS, Wright SJ (2005) Variation in crown light utilization characteristics among tropical canopy trees. Ann Bot 95:535–547

Larjavaara M, Muller-Landau HC (2010) Rethinking the value of high wood density. Funct Ecol 24:701–705

Lefsky MA, Cohen WB, Acker SA, Parker GG, Spies TA, Harding D (1999a) Lidar remote sensing of the canopy structure and biophysical properties of Douglas-fir western hemlock forests. Remote Sens Environ 70:339–361

Lefsky MA, Harding D, Cohen WB, Parker G, Shugart HH (1999b) Surface lidar remote sensing of basal area and biomass in deciduous forests of eastern Maryland, USA. Remote Sens Environ 67:83–98

Lefsky MA, Cohen WB, Harding DJ, Parker GG, Acker SA, Gower ST (2002a) Lidar remote sensing of above-ground biomass in three biomes. Glob Ecol Biogeogr 11:393–399

Lefsky MA, Cohen WB, Parker GG, Harding DJ (2002b) Lidar remote sensing for ecosystem studies. Bioscience 52:19–30

Lefsky MA et al (2005) Estimates of forest canopy height and aboveground biomass using ICESat. Geophys Res Lett 32:L22S02. doi:10.1029/2005GL023971

Leigh EG Jr, Rand AS, Windsor DM (1982) The ecology of a tropical forest: seasonal rhythms and long term changes. Smithsonian Institution Press, Washington, DC

Mascaro J, Becklund KK, Hughes RF, Schnitzer SA (2008) Limited native plant regeneration in novel, exotic-dominated forests on Hawai'i. For Ecol Manag 256:593–606

Mascaro J, Asner GP, Muller-Landau HC, van Breugal M, Hall J, Dahlin K (2011a) Controls over aboveground forest carbon density on Barro Colorado Island, Panama. Biogeosciences 8:1615–1629

Mascaro J, Detto M, Asner GP, Muller-Landau HC (2011b) Evaluating uncertainty in mapping carbon with airborne LiDAR. Remote Sens Environ. doi:10.1016/j.rse.2011.07.019

Means JE et al (1999) Use of large-footprint scanning airborne lidar to estimate forest stand characteristics in the Western Cascades of Oregon. Remote Sens Environ 67:298–308

Niklas KJ (2006) A phyletic perspective on the allometry of plant biomass-partitioning patterns and functionally equivalent organ-categories. New Phytol 171:27–40

Popescu SC, Wynne RH, Scrivani JA (2004) Fusion of small-footprint lidar and multispectral data to estimate plot-level volume and biomass in deciduous and pine forests in Virginia, USA. For Sci 50:551–565

Reyes G, Brown S, Chapman J, Lugo AE (1992) Wood densities of tropical tree species. USDA Forest Service, New Orleans, p 18

Richards PW (1952) The tropical rainforest. Cambridge University Press, Cambridge

Richards P, Williamson GB (1975) Treefalls and patterns of understory species in a wet lowland tropical forest. Ecology 56:1226–1229

Schimel DS (1995) Terrestrial ecosystems and the carbon cycle. Glob Change Biol 1:77–91

Schnitzer SA, Bongers F (2011) Increasing liana abundance and biomass in tropical forests: emerging patterns and putative mechanisms. Ecol Lett 14:397–406

Stegen JC, Swenson NG, Valencia R, Enquist BJ, Thompson J (2009) Above-ground forest biomass is not consistently related to wood density in tropical forests. Glob Ecol Biogeogr 18:617–625

ter Steege H et al (2006) Continental-scale patterns of canopy tree composition and function across Amazonia. Nature 443:444–447

Turner BL, Engelbrecht BMJ (2011) Soil organic phosphorus in lowland tropical rain forests. Biogeochemistry 103:297–315

Vieilledent G et al (2011) A universal appraoch to estaimte biomass and carbon stock in tropical forests using generic allometric models. Ecol Appl. doi:10.1890/11-0039.1

Wagner WL, Herbst DR, Sohmer SH (1999) Manual of the flowering plants of Hawai'i. University of Hawaii Press and Bishop Museum Press, Honolulu

Zanne AE et al (2009) Data from: Towards a worldwide wood economics spectrum. Dryad Digital Repository. http://datadryad.org/handle/10255/dryad.235. doi:10.5061/dryad.234